

# Tunneling conductance through gapped bilayer graphene junctions

Nadia Benlakhoy,<sup>1,\*</sup> Ahmed Jellal,<sup>1,2,†</sup> and El Houssine Atmani<sup>3</sup>

<sup>1</sup>Laboratory of Theoretical Physics, Faculty of Sciences,  
Chouaib Doukkali University, PO Box 20, 24000 El Jadida, Morocco

<sup>2</sup>Canadian Quantum Research Center, 204-3002 32 Ave Vernon, BC V1T 2L7, Canada

<sup>3</sup>Laboratory of Nanostructures and Advanced Materials, Mechanics and Thermo fluids,  
Faculty of Sciences and Techniques, Hassan II University, Mohammedia, Morocco

(Dated: October 14, 2022)

The conductance through single-layer graphene (SLG) and AA/AB-stacked bilayer graphene (BLG) junctions is obtained by taking into account band gap and bias voltage terms. First, we consider gapped SLG, while in between, they are connected into pristine BLG. For Fermi energy larger than the interlayer hopping, the conductance as a function of the bilayer region length  $d$  reveals two different models of anti-resonances with the same period. As a function of the band gap, with AA-BLG stacking, the results show that the conductance has the same minima whatever the value of  $d$ , and for AB-BLG,  $d$  remains relevant such that the system creates a global energy gap. Second, we consider pristine SLG, and in between, they are connected to gapped-biased BLG. We observe the appearance of peaks in the conductance profile with different periods and shapes, and also the presence of Klein tunneling with zero conductance in contrast to the first configuration. When  $d$  is less than 10,  $G(E)$  vanishes and exhibits anti-Klein tunneling as a function of the Fermi energy  $E$ . We also investigate the conductance as a function of the bias. For AA-BLG, the results show antiresonances and diminish for a large value of the bias, independently of the bilayer region of length. In contrast, the conductance in AB-BLG has distinct characteristics in that it begins conducting with maxima for small  $E$  and with minima for large  $E$ .

PACS numbers: 73.22.Pr, 72.80.Vp, 73.63.-b

KEYWORDS: Bilayer graphene, junctions, energy gap, transmission, conductance, Klein effect.

## I. INTRODUCTION

After being experimentally isolated, single-layer graphene (SLG) has attracted constantly expanding interest due to its unique characteristics and possible applications [1–3]. Recently, bilayer graphene (BLG) has also been expanded as the next attractive two-dimensional (2D) carbon material [4–7]. As a result of its excellent electronic structure and transport properties [8, 9]. BLG has two different stacking arrangements: AB-BLG and AA-BLG. AB-BLG is the most stable stack that is generally examined theoretically and experimentally [10, 11]. The AA-BLG is just a double copy of SLG, having a linear gapless energy spectrum that has piqued the attention of many theoretical researchers [12, 13].

Recent studies have shown that graphene can create bilayer graphene flakes that are linked to single-layer graphene regions or those with nanoribbon contacts, such as SLG/BLG/SLG interfaces [14–18]. Other studies have examined multiple domain walls that distinguish between numbers of layers [19, 20] or even various stacking types [21, 22]. For example, J. W. González *et al.* [14] evaluate the transport properties of bilayer graphene flakes using armchair nanoribbon contacts. The conductance exhibits oscillations between zero and the maximum value of the conductance. Other theoretical and experimental

research on the transport properties, edge state properties, and appearance of Landau levels in such devices were the main topics [23–27]. Different quantum interference effects in the conductance, such as Fabry-Pérot resonances as well as Fano anti-resonances, have been observed in these systems [16].

In most of these current theoretical studies, the charge carriers behave as transitions among systems with different transport properties. As experimentally observed, at normal incidence, Klein tunneling in SLG yields a probability of 100%. AB-BLG exhibits anti-Klein tunneling using the two-band approximation, and this is due to the conservation of pseudospin [28, 29]. Hence, it is important to examine the tunneling properties of these combined systems in addition to how the transport channels affect the transport properties. We recently [9] investigated the transport properties of a rectangular potential barrier in gapped and biased AB-BLG. We noticed that the conductance is affected, and the anti-Klein tunneling is no longer maintained. Using dielectric materials such as silicon carbide (SiC) [30] or hexagonal boron nitride (h-BN) [31], as well as applying an external electric field [32], it is possible to experimentally realize the band gap  $\Delta$ .

We study the transport properties of SLG, AA-BLG, and AB-BLG junctions that can be created from the blocks shown in Fig. 1. Assume an electron with energy  $E$  goes from left to right, then the first configuration considered here consists of a gapped SLG while in between they are connected into an AB-BLG or AA-BLG stack. We will call it SLG +  $\Delta$ /AA-BLG/SLG +  $\Delta$ ,

\* benlakhoy.n@ucd.ac.ma

† a.jellal@ucd.ac.ma

and SLG +  $\Delta$ /AB-BLG/SLG +  $\Delta$ , as shown in Fig. 1 (a). The second configuration consists of a pristine SLG while in between they are connected to a gapped and biased AB-BLG or AA-BLG stack. This configuration will be referred to as SLG/AA-BLG +  $(\Delta, \delta)$ /SLG, and SLG/AB-BLG +  $(\Delta, \delta)$ /SLG, as shown in Fig. 1 (b). In [14] studies, they examined similar configurations in pristine cases. Our findings are consistent with their results within the respective limits, but we extend them by taking into account the presence of an energy gap. This will be accomplished by taking into account  $\Delta$  in SLG and  $(\Delta, \delta)$  in BLG for a range of Fermi energy and bilayer region length  $d$ . Furthermore, we calculate the conductance as a function of the energy gap. This is important since it shows new results and also the experimentally observable signatures of the new physics, like measuring the interlayer hopping in bilayer graphene. Our main results can be summarized as follows:

For SLG +  $\Delta$ /AA-BLG/SLG +  $\Delta$  the transmission throughout the system shows anti-resonance due to interference from two scattered channels. The conductance as a function of the length  $d$  oscillates with two distinct periods at a fixed energy  $E = 0.5\gamma_1$  and exhibits anti-Klein tunneling due to the presence of  $\Delta$ . Now, fixing the energy to  $E = 2\gamma_1$ , the conductance shows one obvious phase. The conductance reveals two distinct patterns of anti-resonances with identical periods when the energy is slightly increased to  $2.5\gamma_1$ . The conductance oscillates for SLG +  $\Delta$ /AB-BLG/SLG +  $\Delta$  due to finite-size influences. When,  $E = 0.5\gamma_1$  there is no zero-conductance compared to the SLG +  $\Delta$ /AA-BLG/SLG +  $\Delta$  case, but for  $(E = 2\gamma_1, E = 2.5\gamma_1)$  we get anti-resonances with zero conductance. The conductance has different minima as a function of the Fermi energy for each value of the band gap  $\Delta$ , whereas for  $E > \gamma_1$ , the minima of the conductance match for all  $\Delta$  values. As a result, the conductance is determined by the length  $d$  of the bilayer region. As a function of the band gap, the results show that  $G$  has the same minima regardless of the  $d$  value in SLG +  $\Delta$ /AA-BLG/SLG +  $\Delta$ , and  $d$  remains relevant in SLG +  $\Delta$ /AB-BLG/SLG +  $\Delta$   $d$ , resulting in a global energy gap. We show how the band gap and bias affect conductance as a function of  $d$  in the second configuration SLG/(AA-BLG & AB-BLG) +  $(\Delta, \delta)$ /SLG over a wide range of Fermi energies. We observe the appearance of peaks in the conductance profile with different periods and shapes, and also the presence of Klein tunneling with zero-conductance in contrast to the first configuration. For lengths greater than 10, an oscillating dependence appears. However, the conductance disappears and shows anti-Klein tunneling when  $d$  is smaller than 10. We investigate the conductance as a function of the bias  $\delta$ . For SLG/AA-BLG +  $(\Delta, \delta)$ /SLG, the results show anti-resonances for  $\delta < 0.1\gamma_1$ . Furthermore, we observe the conductance steadily decreasing for a large value of the bias regardless of the length of the bilayer region. For  $\Delta = 0.5\gamma_1$ , we get zero conductance with extra peaks in the conductance profile attributed to

the transmitting channels in the AA-BLG. The findings show that the conductance reflects opposite behavior as a function of the interlayer bias and more specifically, the Fermi energy. On the other hand, the conductance of SLG/AB-BLG +  $(\Delta, \delta)$ /SLG configuration has distinct characteristics. It begins to conduct with maxima when  $E = 0.5\gamma_1$  and minima starting from  $E > 0.5\gamma_1$ .

The paper under discussion is organized as follows. In Sec. II, we introduce the full-band continuum model used to describe both configurations. Additionally, we discuss conductance calculations, for which we use the wavefunction correspondence technique. Numerical findings and a discussion of conductance are discussed in Section III. Finally, in Sec. IV, we summarize our main conclusions.

## II. ELECTRONIC MODEL

### A. AA stacking

Bilayer graphene (BLG) consists of two stacked hexagonal monolayers (MLG). As we refer to them,  $A_1$  and  $B_1$  for the layer 1,  $A_2$  and  $B_2$  for the layer 2. For AA stacking, both sublattices of layer 1 are placed directly on top of the two sublattices  $A_2$  and  $B_2$  of layer 2. The intralayer interatomic distance is  $a_0 = 1.42 \text{ \AA}$ , and it is proportional to the lattice constant  $a = \sqrt{3}a_0$  and the interplanar spacing  $c_{AA} = 3.55 \text{ \AA}$ . In the wave function basis  $\psi(x, y) = [\psi_{A_1}(x, y), \psi_{B_1}(x, y), \psi_{A_2}(x, y), \psi_{B_2}(x, y)]^\dagger$ , with  $\dagger$  represents the row vector's transpose, the Hamiltonian, near the valley  $\mathbf{K}$ , can be expressed as [2, 14, 33, 34]

$$\mathcal{H}_{AA} = \begin{pmatrix} 0 & v_F \pi^\dagger & \gamma_1 & 0 \\ v_F \pi & 0 & 0 & \gamma_1 \\ \gamma_1 & 0 & 0 & v_F \pi^\dagger \\ 0 & \gamma_1 & v_F \pi & 0 \end{pmatrix}, \quad (1)$$

where  $v_F = \frac{\gamma_0}{\hbar} \frac{3a_0}{2} \approx 10^6 \text{ m/s}$  is the Fermi velocity for electrons in each graphene layer,  $\gamma_0$  is the intralayer coupling between atoms, with  $\pi = p_x + ip_y$  are the in-plan momenta and its conjugate with  $p_{x,y} = -i\hbar\partial_{x,y}$ .  $\gamma_1$  is the interlayer coupling term, in our case we take just  $\gamma_1 = 0.266 \text{ eV}$ , in conformity with the experimental findings [10, 35]. Despite the fact that the other interlayer terms have a small impact on transmission [8]. Two different interactions will be introduced to pristine AA-BLG, both referring to an energy gap [36, 37] a band gap  $\Delta$ , and interlayer bias term  $\delta$  given by

$$\mathcal{H}_\Delta = \text{Diag}\{\Delta, -\Delta, \Delta, -\Delta\}, \quad (2)$$

$$\mathcal{H}_\delta = \text{Diag}\{\delta, \delta, -\delta, -\delta\}, \quad (3)$$

in which the total Hamiltonian becomes

$$\mathcal{H} = \mathcal{H}_{AA} + \mathcal{H}_\Delta + \mathcal{H}_\delta. \quad (4)$$

Because momentum in the  $y$  direction is conserved due to translational invariance in that direction, we decompose the spinor as

$$\psi(x, y) = e^{ik_y y} [\phi_{A_1}, \phi_{B_1}, \phi_{A_2}, \phi_{B_2}]. \quad (5)$$

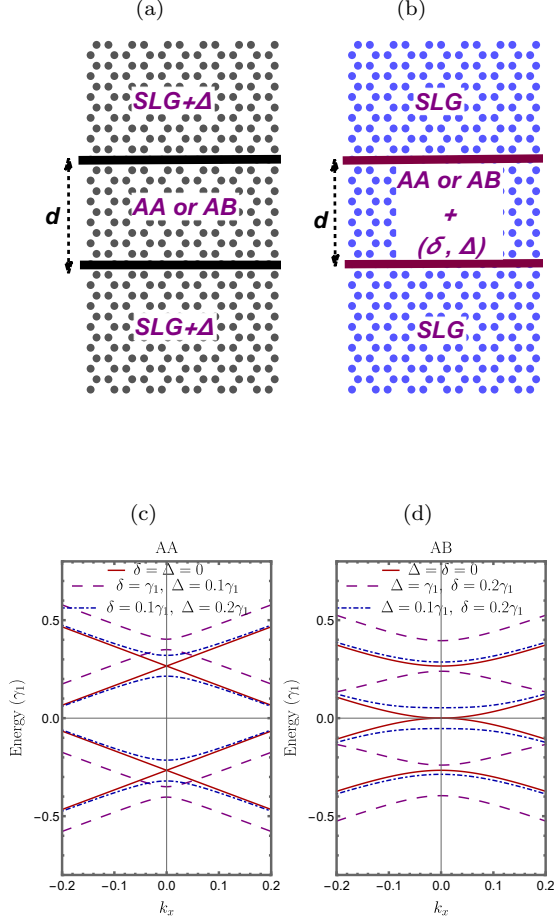


FIG. 1. (Color online) Two different geometries for bilayer and single graphene layer interfaces. (a) AA or AB bilayer graphene sandwiched between gapped single layer graphene: (SLG + Δ/AA-BLG/SLG + Δ, SLG + Δ/AB-BLG/SLG + Δ). (b) Gapped AA or gapped AB bilayer graphene sandwiched between pristine single layer graphene SLG/AA-BLG + (Δ, δ)/SLG, and SLG/AB-BLG + (Δ, δ)/SLG. Energy spectrum for AA (c) and AB (d) for various values of δ and Δ.

Then, using the Schrodinger equation  $\mathcal{H}\psi = E\psi$ , we get four linked differential equations

$$-i[\partial_x + k_y]\phi_{B_1} + \gamma_1\phi_{A_2} = (E - \Delta - \delta)\phi_{A_1}, \quad (6)$$

$$-i[\partial_x - k_y]\phi_{A_1} + \gamma_1\phi_{B_2} = (E + \Delta - \delta)\phi_{B_1}, \quad (7)$$

$$-i[\partial_x + k_y]\phi_{B_2} + \gamma_1\phi_{A_1} = (E - \Delta + \delta)\phi_{A_2}, \quad (8)$$

$$-i[\partial_x - k_y]\phi_{A_2} + \gamma_1\phi_{B_1} = (E + \Delta + \delta)\phi_{B_2}. \quad (9)$$

The set (6-9) can be simplified to a single second-order differential equation for  $\phi_{B_1}$ , as shown below

$$[\partial_x^2 + (k_x^\pm)^2]\phi_{B_1} = 0, \quad (10)$$

with the wave vectors

$$k_x^\pm = \sqrt{-k_y^2 + \varepsilon^2 + \beta^2 + \gamma_1^2 \pm 2\varepsilon\lambda}, \quad (11)$$

where  $\beta = \sqrt{\delta^2 - \Delta^2}$ , and  $\lambda = \sqrt{\gamma_1^2 + \delta^2}$ . The energy spectrum for the system is provided by Eq. (11), which

follows that

$$E_{s'}^s = s' \sqrt{k^2 + \tau^2 + \gamma_1^2 + s\sqrt{\lambda(k^2 + \Delta^2)}}, \quad (12)$$

where  $s, s' = \pm$ ,  $\tau = \sqrt{\delta^2 + \Delta^2}$ , and  $k = \sqrt{k_x^2 + k_y^2}$ .

## B. AB stacking

In the case of AB-BLG, we considered the Bernal stacking [38], which means that the two sublattices  $A_1$  is precisely on top of the sublattice  $B_2$ . The associated Hamiltonian is given by

$$\mathcal{H} = \mathcal{H}_{AB} + \mathcal{H}_\Delta + \mathcal{H}_\delta. \quad (13)$$

Following the same steps as AA-stacking, we find the energy spectrum of AB-BLG as

$$E_{s'}^s = s' \left[ k^2 + \tau^2 + \frac{\gamma_1^2}{2} + s\sqrt{k^2(\gamma_1^2 + 4\delta^2) + \left(\frac{\gamma_1^2}{2} + 2\delta\Delta\right)^2} \right]^{\frac{1}{2}}. \quad (14)$$

For the corresponding propagating modes in AB-BLG, there are two labeled by  $k^+$  and  $k^-$ . They are

$$k^\pm = \sqrt{-k_y^2 + E^2 + \beta \pm \sqrt{E^2(\gamma_1^2 + 4\delta^2) - \gamma_1^2(\delta - \Delta)^2}}. \quad (15)$$

In Fig. 1 (c,d) we illustrate the energy spectra of the AA-BLG and AB-BLG for various system model parameters. We see that for biased δ and gapped Δ AA-BLG, the two Dirac cones are shifted at the two pairs of values ( $\Delta = \gamma_1, \delta = 0.17\gamma_1$ ) (purple dashed line) and ( $\Delta = 0.1\gamma_1, \delta = 0.3\gamma_1$ ) (blue dot dashed line), whereas the proportionality to  $\gamma_1$  create parabolic cones. The two bands are flipped and located at  $\pm\sqrt{\gamma_1^2 + \beta^2 - 2\delta\Delta}$  for the biased and gapped AB-BLG, and the touching bands are moved apart by  $\delta + \Delta$ .

The transmission, reflection, and the coefficients of the wave functions in the AA-BLG or AB-BLG part are identified by implementing the required boundary conditions starting with  $x = 0$  and finally with  $x = d$  for both regions of AA-BLG or AB-BLG, see Appendix D. Using the transmission probabilities, we can calculate the conductance as a function of the energy given by the Landauer-Buttiker formula

$$G(E) = G_0 T(E), \quad (16)$$

where  $G_0 = 2e^2/h$ .

## III. NUMERICAL RESULTS AND DISCUSSION

### 1. SLG + Δ/AA-BLG & AB-BLG/SLG + Δ

We numerically examine and discuss our main findings for gapped SLG with pristine AA-BLG stacking and pristine AB-BLG stacking, namely SLG + Δ/AA-BLG/SLG + Δ, and SLG + Δ/AB-BLG/SLG + Δ configurations. In Fig. 2, the conductance is plotted as a function of the length  $d$ . Here,

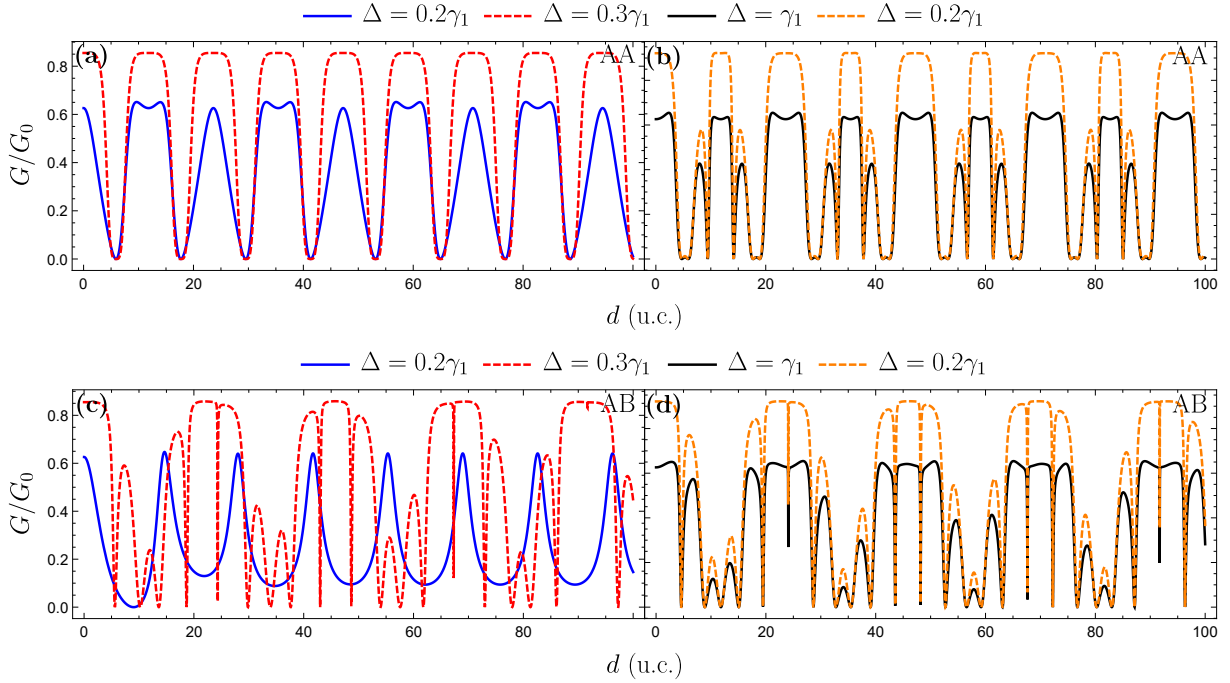


FIG. 2. (Color online) Conductance as a function of bilayer region length  $d$  through SLG +  $\Delta$ /AA-BLG/SLG +  $\Delta$  (top panel) and SLG +  $\Delta$ /AB-BLG/SLG +  $\Delta$  (bottom panel) junctions, with energies  $E = 0.5\gamma_1$  (blue solid lines),  $E = 2\gamma_1$  (red dashed lines), and  $E = 2.5\gamma_1$  (black solid lines and orange solid lines).

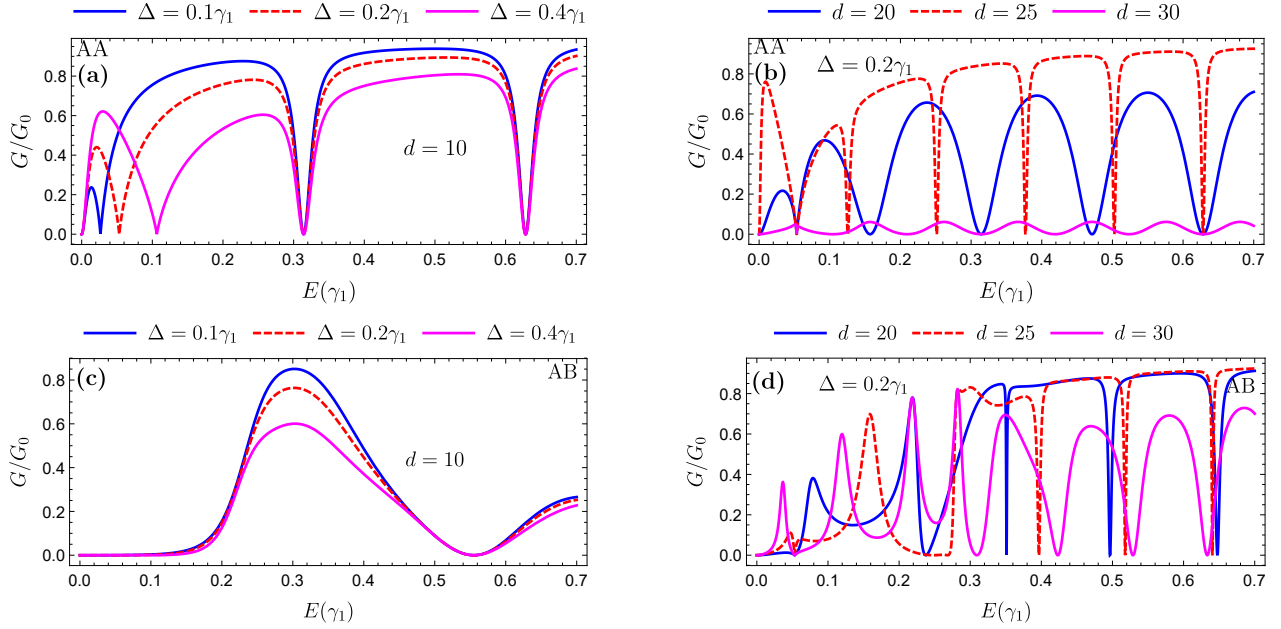


FIG. 3. (Color online) Conductance as a function of the Fermi energy through SLG +  $\Delta$ /AA-BLG/SLG +  $\Delta$ , and SLG +  $\Delta$ /AB-BLG/SLG +  $\Delta$  junctions.

$d$  is expressed in the armchair ribbon (u.c.) length, which is  $3a_0$  [14]. For SLG +  $\Delta$ /AA-BLG/SLG +  $\Delta$  in Fig. 2 (a), the transmission through the system shows anti-resonances due to the interference of two scattered channels. At a fixed energy of  $E = 0.5\gamma_1$  and a band gap of  $\Delta = 0.2\gamma_1$ , the conductance

oscillates with two distinct periods of 24 and 33 u.c. (blue solid line) as a function of length  $d$ . It also exhibits anti-Klein tunneling due to the presence of  $\Delta$ , with one of the periods changing compared to the result obtained in [14]. For  $E = 2\gamma_1$  and  $\Delta = 0.3\gamma_1$ , the conductance shows one obvious



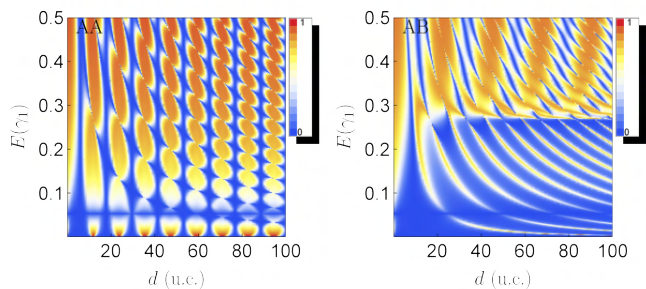


FIG. 4. (Color online) Density plot of the transmission probability as a function of bilayer region length  $d$ , and Fermi energy  $E$  through SLG +  $\Delta$ /AA-BLG/SLG +  $\Delta$ , and SLG +  $\Delta$ /AB-BLG/SLG +  $\Delta$ , with  $\Delta = 0.2\gamma_1$ .

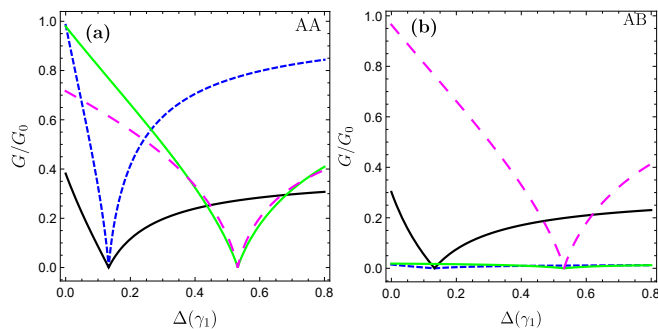


FIG. 5. (Color online) Conductance as a function of the band gap  $\Delta$ , for SLG +  $\Delta$ /AA-BLG/SLG +  $\Delta$ , and SLG +  $\Delta$ /AB-BLG/SLG +  $\Delta$  junctions.  $(E, d) = (0.5\gamma_1, 10)$  (blue dashed line),  $(E, d) = (0.5\gamma_1, 20)$  (black solid line),  $(E, d) = (2\gamma_1, 10)$  (magenta dashed line),  $(E, d) = (2\gamma_1, 20)$  (blue dashed line).

phase of 4 u.c. As in Fig. 2 (b) for  $2.5\gamma_1$  with  $\Delta = \gamma_1$  (black solid line) and  $\Delta = 0.2\gamma_1$  (orange dashed line), the conductance reveals two different patterns of anti-resonances with identical periods of 23 u.c. We plotted the conductance for SLG +  $\Delta$ /AB-BLG/SLG +  $\Delta$  as a function of length  $d$  in Fig. 2 (c). For  $E = 0.5\gamma_1$  and  $\Delta = 0.2\gamma_1$  (blue solid line), there is just one transmission channel in the AB-BLG. Indeed, there are no anti-resonances in this energy; the conductance oscillates as a consequence of finite-size influences. These are also known as Fabry-Pérot resonances [39]. In this case, the presence of our band gap  $\Delta$  reduces conductance, but there is no zero-conductance as in the SLG +  $\Delta$ /AA-BLG/SLG +  $\Delta$  case. For energies greater than  $\gamma_1$  ( $E = 2\gamma_1$ ,  $E = 2.5\gamma_1$ ), Fig. 2 (d), both configurations have two propagation channels. The case here has been updated, and it now shows anti-resonances with zero conductance. In this case, the anti-resonances have periods that depend on  $E$ ,  $\gamma_1$ ,  $d$ , and the band gap  $\Delta$ . This remarkable distinction against the AA case is due to the fact that all atoms are connected in the AA pattern, but only half of the atoms in the AB case are linked by interlayer hopping as noted in [14].

The conductance  $G(E)$  for the gapped SLG as a function of the Fermi energy is shown in Fig. 3 for the two investigated geometries with  $d = 10$  on the left panel and  $d = (20, 25, 30)$  on the right panel. Regarding the first

SLG +  $\Delta$ /AA-BLG/SLG +  $\Delta$  case plotted in Fig. 3 (a), the conductance shows different minima for each value of the band gap for  $E < \gamma_1$ . In contrast to  $E > \gamma_1$ , the conductance minima match for all values of  $\Delta = (0.1\gamma_1, 0.2\gamma_1, 0.4\gamma_1)$ . The SLG +  $\Delta$ /AB-BLG/SLG +  $\Delta$  case is shown in Fig. 3 (c), and the conductance is zero in the energy range  $(0, \gamma_1)$  for  $d = 10$ . Fixing now  $\delta$  for  $0.2\gamma_1$  and prolonging the bilayer region length  $d$ , the additional peaks that can be seen in the conductance pattern in SLG +  $\Delta$ /AA-BLG/SLG +  $\Delta$  are associated with Fano anti-resonances with zero conductance, and in the SLG +  $\Delta$ /AB-BLG/SLG +  $\Delta$  are associated with Fabry-Pérot-resonances. It is worth noting that the conductance depends on  $d$  and obviously varies from 0 when  $d > 25$  through SLG +  $\Delta$ /AA-BLG/SLG +  $\Delta$  as shown in Fig. 3 (b).

The density plot of the transmission probability as a function of Fermi energy and a bilayer region of length  $d$  for  $\Delta = 0.2\gamma_1$  at normal incidence ( $k_y = 0$ ) is shown in Fig. 4. There are two distinct energy regimes based on interlayer coupling. There are no anti-resonances in SLG +  $\Delta$ /AA-BLG/SLG +  $\Delta$  due to the presence of two transmitting modes, as opposed to SLG +  $\Delta$ /AB-BLG/SLG +  $\Delta$ , which has only one propagating mode. The implication is that for various values of  $d$ , even after the band gap is taken into account, the conductance is zero, regardless of the energy or  $\delta$ . We guarantee the fact that this property can be utilized to quantify the interlayer hopping parameter since the period relies primarily on the  $\gamma_1$  parameter.

To investigate the effect of the band gap  $\Delta$ , we show in Fig. 5 the conductance through SLG +  $\Delta$ /AA-BLG/SLG +  $\Delta$ , and SLG +  $\Delta$ /AB-BLG/SLG +  $\Delta$  junctions at normal incidence as a function of  $\Delta$  for various Fermi energies and bilayer length  $d$ . For SLG +  $\Delta$ /AA-BLG/SLG +  $\Delta$  plotted in Fig. 5 (a), the results show that whatever the value of  $d$ , the conductance has the same minima,  $0.13\gamma_1$  for  $E = 0.5\gamma_1$  (blue dashed line, black solid line) and  $0.53\gamma_1$  for  $E = 2\gamma_1$  (purple dashed line, green solid line). The SLG +  $\Delta$ /AB-BLG/SLG +  $\Delta$  case is shown in Fig. 5 (b). When  $d \leq 10$  and for  $E < \gamma_1$  or  $E > \gamma_1$ , conductance remains 0 for all  $\Delta$ . We conclude that the bilayer region length  $d$  remains relevant such that the system creates a global energy gap.

## 2. SLG/(AA-BLG & AB-BLG) + $(\Delta, \delta)$ /SLG

We present charge carriers tunneling through SLG/AA-BLG +  $(\Delta, \delta)$ /SLG, and SLG/AB-BLG +  $(\Delta, \delta)$ /SLG systems. The influence of the band gap  $\Delta = 0.1\gamma_1$  and the bias  $\delta = 0.2\gamma_1$  on the conductance as a function of the bilayer region of length  $d$  for a range of Fermi energy  $E = (0.5\gamma_1, 2\gamma_1, 3\gamma_1)$  is shown in Fig. 6. We see peaks in the conductance profile with different periods and shapes for both geometries SLG/AA-BLG +  $(\Delta, \delta)$ /SLG and SLG/AB-BLG +  $(\Delta, \delta)$ /SLG. The presence of Klein tunneling with zero-conductance in contrast to the first case (see Fig. 2). The Klein tunneling becomes attainable if certain parameters are fulfilled, as outlined recently in [40]. The presence of resonances in the SLG/AB-BLG +  $(\Delta, \delta)$ /SLG case can be explained by the presence of charge carriers with different chiralities and the finite size of the AB-BLG, which also corresponds to our recent work [9].

The conductance  $G(E)$  as a function of the Fermi energy is shown in Figs. 7 (a,b) for two values of the length  $d = 10$  (blue solid line), and  $d = 20$  (magenta dashed line)

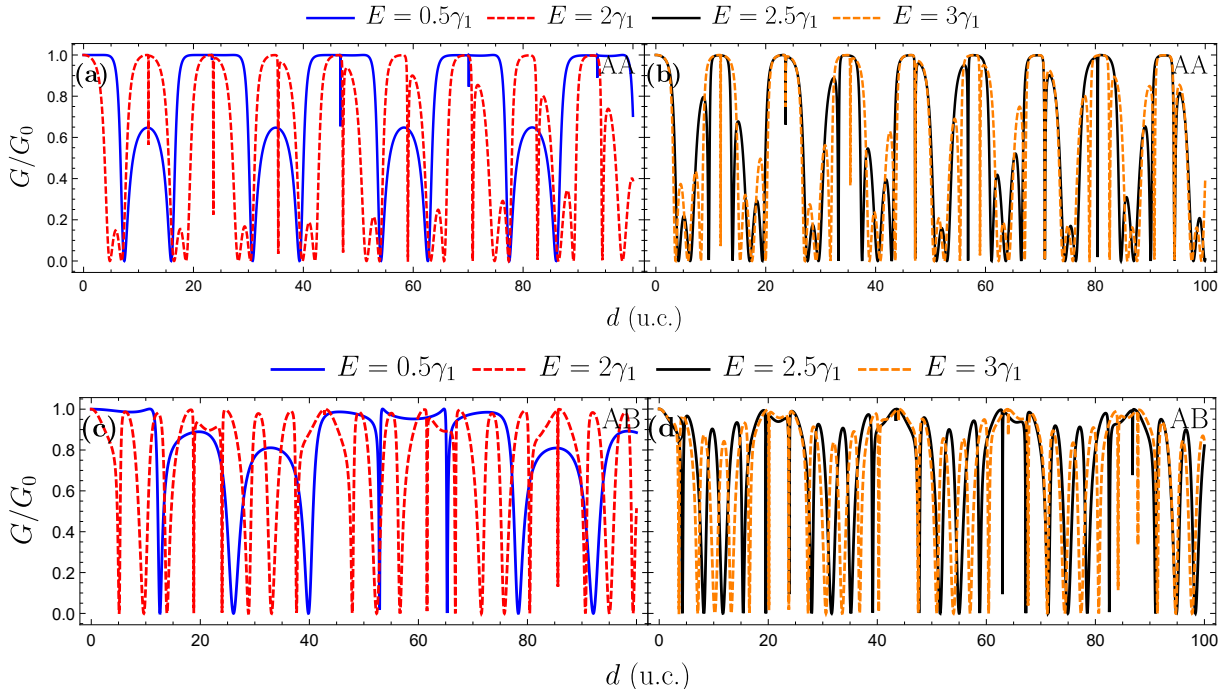


FIG. 6. (Color online) Conductance as a function of bilayer region length  $d$  through SLG/AA-BLG +  $(\Delta, \delta)$ /SLG, and SLG/AB-BLG +  $(\Delta, \delta)$ /SLG junctions, with  $\delta = 0.2\gamma_1$  and  $\Delta = 0.1\gamma_1$ .

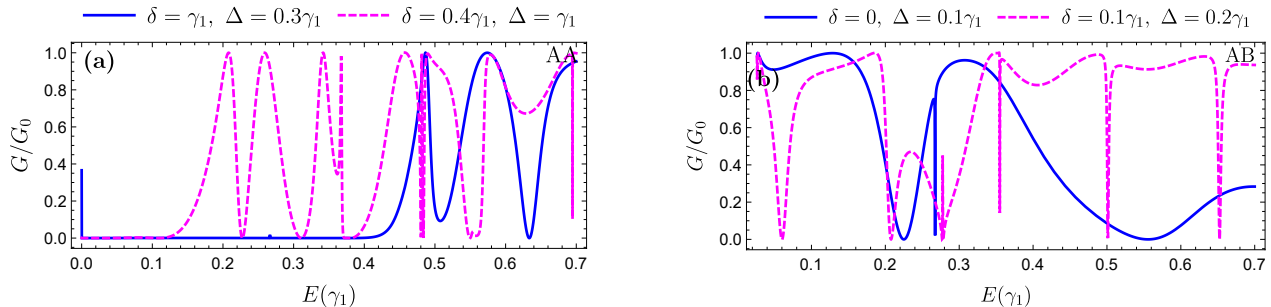


FIG. 7. (Color online) Conductance as a function of the Fermi energy through (a) SLG/AA-BLG +  $(\Delta, \delta)$ /SLG, and (b) SLG/AB-BLG +  $(\Delta, \delta)$ /SLG junctions, with  $d = 10$  (blue solid line), and  $d = 20$  (magenta dashed line).

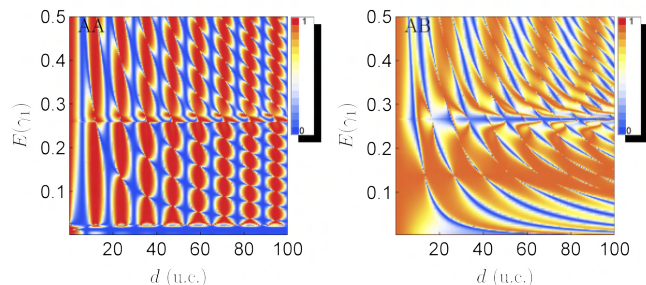


FIG. 8. (Color online) Density plot of the transmission probability as a function of bilayer region of length  $d$ , and Fermi energy  $E$  through SLG/AA-BLG +  $(\Delta, \delta)$ /SLG, and SLG/AB-BLG +  $(\Delta, \delta)$ /SLG junctions, with parameters  $\delta = 0.02\gamma_1$ , and  $\Delta = 0.03\gamma_1$ .

with bias for SLG/AA-BLG +  $(\Delta, \delta)$ /SLG and without bias for SLG/AB-BLG +  $(\Delta, \delta)$ /SLG with  $d = 10$ . An oscillating dependence between the conductance  $G$  and lengths larger than 10 is apparent. However, as depicted in the figures, the conductance vanishes and shows anti-Klein tunneling when  $d$  is smaller than 10. The density plot of transmission probability  $T$  as a function of bilayer region length  $d$  and Fermi energy  $E$  through SLG/AA-BLG +  $(\Delta, \delta)$ /SLG, and SLG/AB-BLG +  $(\Delta, \delta)$ /SLG junctions is shown in Fig. 8. The presence of a biased potential  $\delta$  and a band gap  $\Delta$  can significantly alter  $T$ . Around  $E = 0.25\gamma_1$ ,  $T$  becomes asymmetric and strongly suppressed for low Fermi energy  $E$ . This is due to the fact that with an increase of the two parameters  $\delta$  and  $\Delta$ , the Dirac electron can be controlled within a finite region in both configurations [41].

In Fig. 9, we show the conductance in SLG/AA-BLG +  $(\Delta, \delta)$ /SLG as a function of the bias with (a,b,c) for  $E = 0.5\gamma_1$

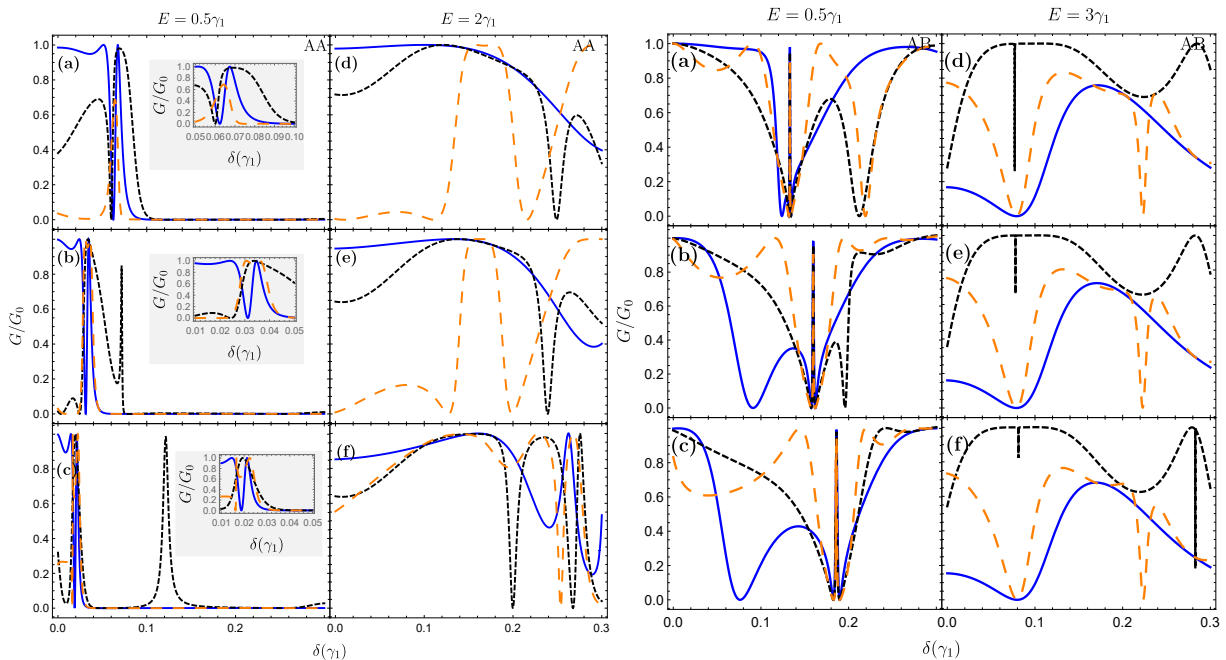


FIG. 9. (Color online) Conductance for SLG/AA-BLG +  $(\Delta, \delta)$ /SLG, and SLG/AB-BLG +  $(\Delta, \delta)$ /SLG as a function of the bias  $\delta$  for normal incidence, with different value of bilayer region length  $d = 10$  (blue solid line),  $d = 20$  (black dashed line),  $d = 30$  (orange dashed line), and parameters in left panel: (a)  $(E, \Delta) = (0.5\gamma_1, 0)$ , (b)  $(E, \Delta) = (0.5\gamma_1, 0.2\gamma_1)$ , (c)  $(E, \Delta) = (0.5\gamma_1, 0.3\gamma_1)$ , (d)  $(E, \Delta) = (2\gamma_1, 0)$ , (e)  $(E, \Delta) = (2\gamma_1, 0.2\gamma_1)$ , (f)  $(E, \Delta) = (2\gamma_1, 0.3\gamma_1)$ . In the right panel with parameters: (a)  $(E, \Delta) = (0.5\gamma_1, 0)$ , (b)  $(E, \Delta) = (0.5\gamma_1, 0.1\gamma_1)$ , (c)  $(E, \Delta) = (0.5\gamma_1, 0.2\gamma_1)$ , (d)  $(E, \Delta) = (3\gamma_1, 0)$ , (e)  $(E, \Delta) = (3\gamma_1, 0.1\gamma_1)$ , (f)  $(E, \Delta) = (3\gamma_1, 0.2\gamma_1)$ .

and (d,e,f) for  $E = 2\gamma_1$ . The results show anti-resonances for  $\delta < 0.1\gamma_1$  in Fig. 9 (a,b). Furthermore, we see the conductance steadily decreasing for a large bias value independent of the bilayer region length  $d$ . Selecting  $\Delta = 0.5\gamma_1$ , we obtain zero-conductance with extra peaks appearing in the conductance profile with bias attributed to the transmitting channels in AA-BLG, see Fig. 9 (c). Fig. 9 (d,e,f) depict clear anti-resonances. The findings show that the conductance reflects opposite behavior as a function of the inter-layer bias and more specifically, the Fermi energy. The conductance through SLG/AB-BLG +  $(\Delta, \delta)$ /SLG case has distinct characteristics, it starts conducting with maxima for  $E = 0.5\gamma_1$  and minima for  $E = 3\gamma_1$ , as shown in Fig. 9 (right panel).

#### IV. CONCLUSION

We have studied the conductance through single-layer graphene (SLG), and bilayer graphene (BLG) junctions, taking into account band gap  $(\Delta)$  and bias  $(\delta)$  voltage terms. We started with gapped SLG with perfect AA/AB-BLG (SLG +

$\Delta$ /AA-BLG/SLG +  $\Delta$ ), and (SLG +  $\Delta$ /AB-BLG/SLG +  $\Delta$ ). We have shown that for Fermi energy larger than the inter-layer hopping, the conductance as a function of the bilayer region of length reveals two different models of anti-resonances with the same period. As a function of the band gap, in AA-BLG stacking, the results show that the conductance has the same minima whatever the value of  $d$ , and for AB-BLG,  $d$  remains relevant such that the system creates a global energy gap.

In the second configuration, we considered pristine SLG and gapped-biased BLG (SLG/AA-BLG +  $(\Delta, \delta)$ /SLG), and (SLG/AB-BLG +  $(\Delta, \delta)$ /SLG). We found the appearance of peaks in the conductance profile with different periods and shapes, and also the presence of Klein tunneling with zero conductance in contrast to the first configuration. When  $d$  is less than 10, the conductance  $G(E)$  vanishes and exhibits anti-Klein tunneling as a function of the Fermi energy  $E$ . We have also evaluated the conductance as a function of the bias. For AA-BLG, the results show antiresonances and diminish for a large value of the bias independent of the bilayer region of length. On the other hand, in AB-BLG, conductance has distinct characteristics.

[1] Kostya S Novoselov, Andre K Geim, Sergei V Morozov, De-eng Jiang, Yanshui Zhang, Sergey V Dubonos, Irina V Grigorieva, and Alexandr A Firsov. Electric field effect in atomically thin carbon films. *science*, 306(5696):666–669,

2004.

[2] AH Castro Neto, Francisco Guinea, Nuno MR Peres, Kostya S Novoselov, and Andre K Geim. The electronic properties of graphene. *Reviews of modern physics*,

- 81(1):109, 2009.
- [3] Rahul Raveendran Nair, Peter Blake, Alexander N Grigorenko, Konstantin S Novoselov, Tim J Booth, Tobias Stauber, Nuno MR Peres, and Andre K Geim. Fine structure constant defines visual transparency of graphene. *science*, 320(5881):1308–1308, 2008.
  - [4] Edward McCann and Vladimir I Fal’ko. Landau-level degeneracy and quantum hall effect in a graphite bilayer. *Physical review letters*, 96(8):086805, 2006.
  - [5] F Guinea, AH Castro Neto, and NMR Peres. Electronic states and landau levels in graphene stacks. *Physical Review B*, 73(24):245426, 2006.
  - [6] H-V Roy, C Kallinger, and K Sattler. Study of single and multiple foldings of graphitic sheets. *Surface science*, 407(1-3):1–6, 1998.
  - [7] Eduardo V Castro, KS Novoselov, SV Morozov, NMR Peres, JMB Lopes Dos Santos, Johan Nilsson, F Guinea, AK Geim, and AH Castro Neto. Biased bilayer graphene: semiconductor with a gap tunable by the electric field effect. *Physical review letters*, 99(21):216802, 2007.
  - [8] B Van Duppen and FM Peeters. Four-band tunneling in bilayer graphene. *Physical Review B*, 87(20):205427, 2013.
  - [9] Nadia Benlakhrouy, Abderrahim El Mouhafid, and Ahmed Jellal. Transport properties in gapped bilayer graphene. *Physica E: Low-dimensional Systems and Nanostructures*, 134:114835, 2021.
  - [10] Taisuke Ohta, Aaron Bostwick, Thomas Seyller, Karsten Horn, and Eli Rotenberg. Controlling the electronic structure of bilayer graphene. *Science*, 313(5789):951–954, 2006.
  - [11] MO Goerbig. Electronic properties of graphene in a strong magnetic field. *Reviews of Modern Physics*, 83(4):1193, 2011.
  - [12] AL Rakhmanov, AV Rozhkov, AO Sboychakov, and Franco Nori. Instabilities of the a a-stacked graphene bilayer. *Physical Review Letters*, 109(20):206801, 2012.
  - [13] Chih-Wei Chiu, Szu-Chao Chen, Yuan-Cheng Huang, Feng-Lin Shyu, and Ming-Fa Lin. Critical optical properties of aa-stacked multilayer graphenes. *Applied Physics Letters*, 103(4):041907, 2013.
  - [14] John W González, Hernán Santos, Mónica Pacheco, Leonor Chico, and Luis Brey. Electronic transport through bilayer graphene flakes. *Physical Review B*, 81(19):195406, 2010.
  - [15] Bhagawan Sahu, Hongki Min, and Sanjay K Banerjee. Effects of magnetism and electric field on the energy gap of bilayer graphene nanoflakes. *Physical Review B*, 81(4):045414, 2010.
  - [16] D Zambrano, L Rosales, A Latgé, M Pacheco, and PA Orellana. Photon-assisted transport in bilayer graphene flakes. *Physical Review B*, 95(3):035412, 2017.
  - [17] Wei Yan, Si-Yu Li, Long-Jing Yin, Jia-Bin Qiao, Jia-Cai Nie, and Lin He. Spatially resolving unconventional interface landau quantization in a graphene monolayer-bilayer planar junction. *Physical Review B*, 93(19):195408, 2016.
  - [18] Kendal W Clark, X-G Zhang, Gong Gu, Jewook Park, Guowei He, Randall M Feenstra, and An-Ping Li. Energy gap induced by Friedel oscillations manifested as transport asymmetry at monolayer-bilayer graphene boundaries. *Physical Review X*, 4(1):011021, 2014.
  - [19] F Giannazzo, I Deretzis, A La Magna, F Roccaforte, and Rositsa Yakimova. Electronic transport at monolayer-bilayer junctions in epitaxial graphene on SiC. *Physical Review B*, 86(23):235422, 2012.
  - [20] Babak Zare Rameshti, Malek Zareyan, and Ali G Moghaddam. Supercurrent reversal in Josephson junctions based on bilayer graphene flakes. *Physical Review B*, 92(8):085403, 2015.
  - [21] Marta Pelc, Włodzimierz Jaskólski, Andres Ayuela, and Leonor Chico. Topologically confined states at corrugations of gated bilayer graphene. *Physical Review B*, 92(8):085433, 2015.
  - [22] M Mirzakhani, M Zarenia, and FM Peeters. Edge states in gated bilayer-monolayer graphene ribbons and bilayer domain walls. *Journal of Applied Physics*, 123(20):204301, 2018.
  - [23] CP Puls, NE Staley, and Y Liu. Interface states and anomalous quantum oscillations in hybrid graphene structures. *Physical Review B*, 79(23):235415, 2009.
  - [24] Mikito Koshino, Takeshi Nakanishi, and Tsuneya Ando. Interface Landau levels in graphene monolayer-bilayer junctions. *Physical Review B*, 82(20):205436, 2010.
  - [25] Demin Yin, Weihua Liu, Xin Li, Li Geng, Xiaoli Wang, and Pu Huai. Mono-bi-monolayer graphene junction introduced quantum transport channels. *Applied Physics Letters*, 103(17):173519, 2013.
  - [26] Yasumasa Hasegawa and Mahito Kohmoto. Electric-field-induced penetration of edge states at the interface between monolayer and bilayer graphene. *Physical Review B*, 85(12):125430, 2012.
  - [27] Zi-xiang Hu and Wenxin Ding. Edge states at the interface between monolayer and bilayer graphene. *Physics Letters A*, 376(4):610–615, 2012.
  - [28] MI Katsnelson, KS Novoselov, and AK Geim. Chiral tunnelling and the Klein paradox in graphene. *Nature physics*, 2(9):620–625, 2006.
  - [29] N Stander, B Huard, and D Goldhaber-Gordon. Evidence for Klein tunneling in graphene p-n junctions. *Physical review letters*, 102(2):026807, 2009.
  - [30] Alexandr Vladimirovich Rozhkov, AO Sboychakov, AL Rakhmanov, and Franco Nori. Electronic properties of graphene-based bilayer systems. *Physics Reports*, 648:1–104, 2016.
  - [31] Xuechao Zhai and Guojun Jin. Proposal for realizing the quantum spin Hall phase in a gapped graphene bilayer. *Physical Review B*, 93(20):205427, 2016.
  - [32] Yuanbo Zhang, Tsung-Ta Tang, Caglar Girit, Zhao Hao, Michael C Martin, Alex Zettl, Michael F Crommie, Y Ron Shen, and Feng Wang. Direct observation of a widely tunable bandgap in bilayer graphene. *Nature*, 459(7248):820–823, 2009.
  - [33] Luis Brey and HA Fertig. Electronic states of graphene nanoribbons studied with the Dirac equation. *Physical Review B*, 73(23):235411, 2006.
  - [34] Luis Brey and HA Fertig. Edge states and the quantized Hall effect in graphene. *Physical Review B*, 73(19):195408, 2006.
  - [35] LM Malard, J Nilsson, DC Elias, JC Brant, F Plentz, ES Alves, AH Castro Neto, and MA Pimenta. Probing the electronic structure of bilayer graphene by Raman scattering. *Physical Review B*, 76(20):201401, 2007.
  - [36] Edward McCann and Mikito Koshino. The electronic properties of bilayer graphene. *Reports on Progress in physics*, 76(5):056503, 2013.
  - [37] Sonja Predin, Paul Wenk, and John Schliemann. Trigonal warping in bilayer graphene: Energy versus entanglement spectrum. *Physical Review B*, 93(11):115106, 2016.



- [38] John Desmond Bernal. The structure of graphite. *Proceedings of the Royal Society of London. Series A, Containing Papers of a Mathematical and Physical Character*, 106(740):749–773, 1924.
- [39] I Snyman and CWJ Beenakker. Ballistic transmission through a graphene bilayer. *Physical Review B*, 75(4):045322, 2007.
- [40] B Van Duppen and FM Peeters. Klein paradox for a pn junction in multilayer graphene. *EPL (Europhysics Letters)*, 102(2):27001, 2013.
- [41] Dali Wang and Guojun Jin. Tunable electronic transport characteristics through an aa-stacked bilayer graphene with magnetoelectric barriers. *Journal of Applied Physics*, 112(5):053714, 2012.

## Appendix A: Gapped single layer graphene

The eigenfunctions of the gapped SLG Hamiltonian are given by

$$\psi(x, y) = \mathcal{G}_{\text{SLG}} \mathcal{M}(x) \mathcal{C} e^{ik_y y}, \quad (\text{A1})$$

where

$$\mathcal{G}_{\text{SLG}} = \begin{pmatrix} \alpha^- & -\alpha^+ \\ 1 & 1 \end{pmatrix}, \quad \mathcal{M}(x) = \begin{pmatrix} e^{ik_x} \\ e^{-ik_x} \end{pmatrix}, \quad \mathcal{C} = \begin{pmatrix} a \\ b \end{pmatrix}, \quad (\text{A2})$$

and

$$k_x = \sqrt{E^2 - \Delta^2 - k_y^2}, \quad \alpha^\pm = \frac{k_x \pm ik_y}{E - \Delta}. \quad (\text{A3})$$

## Appendix B: AA-Wavefunction

We demonstrate that the solution to Eq. (10) is a plane wave formed by

$$\phi_{A_1} = a_1 e^{ik^+ x} + a_2 e^{-ik^+ x} + a_3 e^{ik^- x} + a_4 e^{-ik^- x}, \quad (\text{B1})$$

where  $a_n$  are the coefficients of normalization, with  $n = 1, 2, 3, 4$ . The rest of the spinor components can be obtained by substituting this into equations (6-9). The system's wave function can be expressed in matrix form as

$$\psi(x, y) = \mathcal{G}_{\text{AA}} \mathcal{M}(x) \mathcal{C} e^{ik_y y}, \quad (\text{B2})$$

where

$$\mathcal{M}(x) = \begin{pmatrix} e^{ik^+ x} & 0 & 0 & 0 \\ 0 & e^{-ik^+ x} & 0 & 0 \\ 0 & 0 & e^{ik^- x} & 0 \\ 0 & 0 & 0 & e^{-ik^- x} \end{pmatrix}, \quad \mathcal{C} = \begin{pmatrix} a1 \\ a2 \\ a3 \\ a4 \end{pmatrix}, \quad (\text{B3})$$

and

$$\mathcal{G}_{\text{AA}} = \begin{pmatrix} \chi_+^+ & -\chi_-^+ & \chi_+^- & \chi_-^- \\ 1 & 1 & 1 & 1 \\ -\Lambda_+^+ & \Lambda_-^+ & -\Lambda_+^- & \Lambda_-^- \\ \xi_+^+ & \xi_-^+ & \xi_+^- & \xi_-^- \end{pmatrix}, \quad (\text{B4})$$

where

$$\Lambda_\alpha^\pm = \frac{E^2 \delta \pm E \lambda (\delta + \Delta) + \epsilon (\gamma_1^2 \pm E \lambda) + \delta (\delta + \Delta)}{E \gamma_1 (k_x^\pm + \alpha i k_y)}, \quad (\text{B5})$$

$$\xi_\alpha^\pm = \frac{1}{\gamma_1} [E + \Delta - \delta - \alpha (k_x^\pm + i k_y) \chi_\alpha^\pm], \quad (\text{B6})$$

$$\chi_\alpha^\pm = \chi_\alpha^\pm = \frac{1}{E - \Delta - \delta} [k_x^\pm - \alpha i k_y - \gamma_1 \Lambda_\alpha^\pm], \quad (\text{B7})$$

with  $\alpha = \pm$ .

## Appendix C: AB-Wavefunction

The wave function of the system can be written in matrix form as

$$\psi(x, y) = \mathcal{G}_{\text{AB}} \mathcal{M}(x) \mathcal{C} e^{ik_y y}, \quad (\text{C1})$$

where the four-component vector  $\mathcal{C}$  represents the different coefficients, with the matrix  $\mathcal{G}_{\text{AB}}$  given by

$$\mathcal{G}_{\text{AB}} = \begin{pmatrix} \chi_+^+ & \chi_-^+ & \chi_+^- & \chi_-^- \\ 1 & 1 & 1 & 1 \\ -\Lambda_+^+ & \Lambda_-^+ & -\Lambda_+^- & \Lambda_-^- \\ \rho_+^+ & \rho_-^+ & \rho_+^- & \rho_-^- \end{pmatrix}, \quad (\text{C2})$$

and we have set

$$\Lambda_\pm^s = \frac{(k^s \pm i k_y)}{\epsilon - \delta - \Delta}, \quad (\text{C3})$$

$$\rho^\pm = \frac{(\epsilon - \delta - \Delta)(\epsilon - \delta + \Delta) - (k_y)^2 - (k^\pm)^2}{\Gamma_1(\epsilon - \delta - \Delta)}, \quad (\text{C4})$$

$$\xi_\alpha^\pm = \frac{\alpha k^\pm - i k_y}{\epsilon + \delta + \Delta}. \quad (\text{C5})$$

## Appendix D: Wave-function matching

In the configuration adopted, the wave-function is continuous in the bottom layer [2]

$$\begin{cases} \phi_{A_1}(x=0) = \phi_{B_1}(x=0), \\ \phi_{A_2}(x=0) = \phi_{B_2}(x=0) = 0, \\ \phi_{A_1}(x=d) = \phi_{B_1}(x=d), \\ \phi_{A_2}(x=d) = \phi_{B_2}(x=d) = 0. \end{cases} \quad (\text{D1})$$